

# Predicting the QCD critical point and EoS from combining HIC and neutron star observations

Jan Steinheimer,<sup>1,2</sup> Manjunath Omana Kuttan,<sup>2</sup> Tom Reichert,<sup>3,2,4</sup> Yasushi Nara,<sup>5</sup> and Marcus Bleicher<sup>3,1,4</sup>

<sup>1</sup>*GSI Helmholtzzentrum für Schwerionenforschung GmbH, Planckstr. 1, D-64291 Darmstadt, Germany*

<sup>2</sup>*Frankfurt Institute for Advanced Studies (FIAS),*

*Ruth-Moufang-Str. 1, D-60438 Frankfurt am Main, Germany*

<sup>3</sup>*Institut für Theoretische Physik, Goethe-Universität Frankfurt,*

*Max-von-Laue-Str. 1, D-60438 Frankfurt am Main, Germany*

<sup>4</sup>*Helmholtz Research Academy Hesse for FAIR (HFHF),*

*GSI Helmholtzzentrum für Schwerionenforschung GmbH, Campus Frankfurt,*

*Max-von-Laue-Str. 12, 60438 Frankfurt am Main, Germany*

<sup>5</sup>*Akita International University, Yuwa, Akita-city 010-1292, Japan*

A combined constraint on the dense QCD equation of state from connecting neutron star observations to data from heavy ion reactions is presented. We use the Chiral Mean Field Model which can describe neutron star and iso-spin symmetric matter and allows the consistent calculation of the density and momentum dependent potentials of baryons which are then implemented in the UrQMD transport model. In contrast to previous studies, the same equation of state constrained from neutron star properties is also able to describe experimental observables in heavy ion reactions at the HADES experiment.

Quantum-Chromo-Dynamics (QCD) describes the fundamental interaction governing the physics on sub-nuclear scales. Its fundamental properties are usually studied in high energy collider experiments at RHIC or LHC, e.g. with proton+proton reactions or in the collisions of heavy ions. A general feature of reactions at these large collision energies is that the net-baryon density is usually very small and the temperatures (or typical momentum transfers) are very high. Such a scenario was realized in nature a few microseconds after the Big Bang. On the theoretical side, this regime is very favorable, because it allows to probe QCD on the basis of ab-initio calculations or within well controlled perturbative expansions of QCD. Non-perturbative lattice QCD calculations have firmly established a crossover transition from hadronic to partonic matter [1–3].

When going to lower collision energies ( $\sqrt{s_{NN}} < 10$  GeV) the situation becomes dramatically more complicated. In this energy regime one deals with very high net-baryon densities (2-4 times nuclear saturation density  $n_0$ ) and moderate temperatures. This prevents ab-initio lattice QCD calculations due to the well known sign problem and it further prevents many perturbative approaches leaving the study of this regime to effective models of QCD.

Nevertheless, this region of the QCD phase diagram is of great importance and interest. It is speculated that it contains one of the most exciting features of the phase diagram, namely the critical end point, where the chiral crossover transition between the hadron and parton matter changes into a first-order phase transition. The location of the critical end point (CEP) of QCD, or even its existence, is not yet known. Extrapolations of lattice-QCD results have established that the critical end point may only be located at temperatures and baryon chemical potentials above  $\mu_B/T \gtrsim 3$  [4–6]. Current estimates within Dyson-Schwinger and FRG approaches suggest

$T^{CEP} = 80 - 140$  MeV,  $\mu_B^{CEP} = 500 - 800$  MeV [7–10]. This region of  $\mu_B/T \sim 5 - 6$  is similarly favored by Bayesian inference from holographic models [11], Padé type resummations [12, 13], using finite size scaling of net protons cumulants [14] and lattice QCD extrapolations based on contours of constant entropy density [15]. It is the region that is extremely relevant for the understanding of Neutron Stars (NS) and binary NS mergers and it is in the focus of the upcoming (and current) experiments at GSI, FAIR, RHIC-BES, HIAF and FRIB. A direct detection of the critical endpoint is made complicated by the same critical phenomena which define it, namely critical slowing down as well as severe dampening of the critical effects due to finite size and finite lifetime of the systems created in heavy ion reactions [16, 17].

In the present paper we suggest a different route to constraining the phase structure of QCD by combining measurements from neutron star mergers and heavy ion collisions with an effective model for the equation of state.

We will show a very first comparison of simulated results, based on an equation of state constrained from neutron star observations, compared to heavy ion data. Our results will clearly determine whether a simultaneous description of both regimes of dense QCD matter is possible within one equation of state which is an important step towards a combined and conclusive understanding of dense QCD.

## I. THE CMF MODEL AND THE EOS

To be able to combine constraints on the EoS from neutron stars with heavy ion data, a model is required that can provide input for both, based on a limited set of input parameters. For this purpose we will employ the chiral mean field model (CMF) developed in Frankfurt [18–20]. The chiral mean field model is a fully relativistic

parity-doublet approach to describe dense QCD matter, including both the baryonic SU(3)-flavor octet and the  $\Delta$  baryons with their respective parity partners. The model aims to represent an equation of state (EoS) compatible with empirical data from heavy-ion collisions, astrophysical constraints, and lattice QCD simulations. It effectively integrates scalar and vector mean fields, which impact the baryonic masses  $m_{b\pm}^*$  and interactions [21]. The effective baryon mass is then reduced by the light and strange quark scalar fields  $\sigma$ ,  $\zeta$  and reads

$$m_{b\pm}^* = \sqrt{\left[ (g_{\sigma b}^{(1)} \sigma + g_{\zeta b}^{(1)} \zeta)^2 + (m_0 + n_S m_s)^2 \right]} \pm g_{\sigma b}^{(2)} \sigma, \quad (1)$$

in which  $\pm$  stands for positive (negative) parity partners,  $g_i^{(j)}$  are the couplings to the scalar fields,  $n_S$  is the strangeness of the baryon,  $m_0$  represents a bare mass term and  $m_s$  is the current quark mass of the strange quark. The effective chemical potential on the other hand is changed by the vector fields  $\omega$  (net baryon density),  $\rho$  (net iso-spin density),  $\phi$  (net strangeness density) and reads

$$\mu_b^* = \mu_b - g_{\omega b} \omega - g_{\phi b} \phi - g_{\rho b} \rho, \quad (2)$$

where  $g_i$  are the couplings to the vector fields. The mean field values are determined by the scalar and vector interactions. Quark degrees of freedom are incorporated in a PNJL-motivated way having their thermal contribution directly linked to the Polyakov Loop order parameter  $\Phi$  and their effective masses also adjusted by the scalar fields. Finally the model also includes an excluded volume  $v_i$  for baryons and mesons, while quarks are assumed to be point-like. A more detailed description of the model and its implementation in UrQMD, including the momentum dependent potentials, can be found in [22].

While in the previous work [22] the focus was on establishing the UrQMD+CMF model and its implementation, in the following we present a parameter study of the CMF in order to establish whether a simultaneous description of neutron star observables and heavy ion observables is possible, and if yes determine the most suitable parameters.

The parameters which are most relevant for the equation of state as well its momentum dependence are the scalar and vector coupling strengths  $g_\sigma$  and  $g_\omega$  as well as the bare mass of the nucleons  $m_0$ . Note, that these are not entirely independent if one demands that the nucleon vacuum masses are reproduced. By fixing the bare mass  $m_0$  also the momentum dependence of the single particle energy is fixed. In addition to  $g_\omega$ , the repulsive interaction between hadrons can be modified by their excluded volume parameter  $v_i$  and the nuclear incompressibility has been shown to be sensitive to the parameters of the scalar potential. This means we essentially have 4 free parameters in our model but 3 additional constraints, the nuclear saturation density  $n_0 = 0.16 \text{ fm}^{-3}$ , nuclear binding energy per baryon  $E/A - m_N = -16 \text{ MeV}$

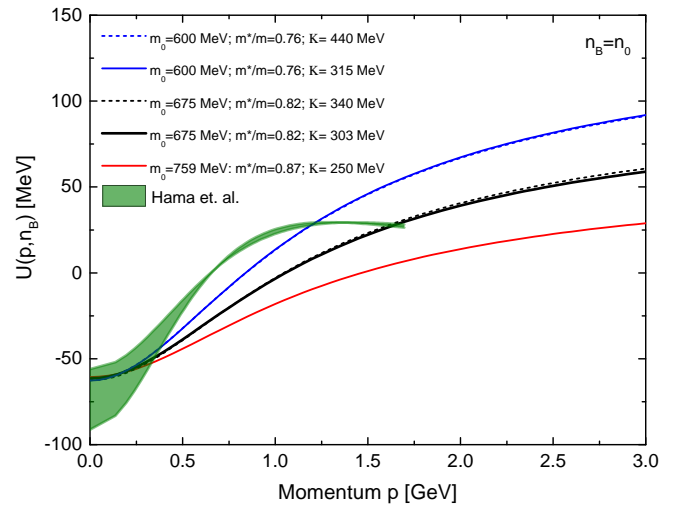


Figure 1. (Color online) Momentum dependence of the single particle potential of nucleons in iso-spin symmetric matter for different parametrizations of the CMF. The green shades area shows momentum dependent Dirac masses extracted from experiment by Hama et.al. [23]

and the incompressibility of nuclear matter at saturation density  $K$ . While the first two can be considered strict constraints, there is some freedom on the incompressibility. In the following we will compare five different parametrizations of the CMF model. The resulting momentum dependencies of the single particle potential  $U(p, n_B)$ , at saturation density, of these 5 scenarios are shown in figure 1. Here, parameter sets with the same bare mass have the same color. For the blue ( $m_0 = 600 \text{ MeV}$ ) and black ( $m_0 = 675 \text{ MeV}$ ) curves also a scenario with increased incompressibility (dashed curves) is shown. As expected, a smaller bare mass, resulting in a stronger scalar coupling, leads to a stronger momentum dependence. At the same time a larger scalar coupling tends to require a stronger vector repulsion to be able to reproduce nuclear binding and saturation properties which leads to a higher incompressibility. Figure 1 lists the effective mass of the nucleon at saturation density for all scenarios. The momentum dependence of the single particle energy derived from proton+nucleus scattering experiments is shown for comparison as green band. This band corresponds to two possible scenarios of the momentum dependence of the relativistic Dirac potential extracted in [23]<sup>1</sup>. For the following comparisons we therefore have 5 different scenarios with 3 different momentum dependencies and a range of incompressibilities.

<sup>1</sup> Note, that also in the QMD part of the UrQMD model we will use the relativistic single particle potential from CMF instead of the Schrödinger equivalent potential [24] as the UrQMD model uses the relativistic kinetic energy and the momentum dependent potential can be understood as an effective way of introducing an effective mass in the relativistic kinetic energy.

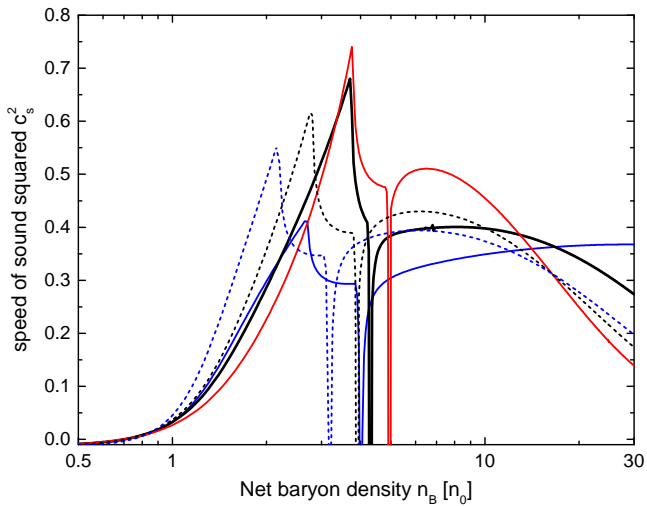


Figure 2. (Color online) Speed of sound squared at  $T = 0$  in iso-spin symmetric matter for the different parametrizations.

The resulting equations of state, represented by the speed of sound as a function of the net baryon density in iso-spin symmetric matter is shown in figure 2. All curves show a characteristic peak of the speed of sound, its position and height depend on the parameters. While scenarios with a large incompressibility show a peak at a rather low density, the height of the peak seems to be systematically lower for a strong momentum dependence. All equations of state show a decrease of the speed of sound below the conformal limit of  $1/3$  due to the appearance of free quarks that start to dominate at high densities.

Using the Tolmann-Oppenheimer-Volkoff (TOV) equation [25], one can relate the equation of state to a unique mass-radius relation of neutron stars. To do so in the CMF model, we perform calculations assuming  $\beta$ -equilibrium matter, including electrons and muons, and omit strangeness conservation. Using the well established DD2 [26] equation of state for the crust (densities below  $0.5 n_0$ ) we obtain five different mass radius curves for the different scenarios. These are shown as lines in figure 3. The colors and styles of the lines are the same as in the previous figures. The green shaded area is a constraint from a binary neutron star merger [27] which is also consistent with NICER constraints [28–33]. As one can see the solid black line gives the best description of the constraint which corresponds to an intermediate momentum dependence and a nuclear incompressibility of  $K = 303$  MeV. In the following we will refer to results with this parametrization as the *best fitting parametrization* and always show it as a black solid line. Using the best fitting parametrization, where  $m_0 = 675$  MeV and  $K = 303$  MeV, we also calculated the symmetry energy  $E_{sym} = 31$  MeV and slope of the symmetry energy  $L = 53$  MeV, which are both well within the range of experimental observations [34].

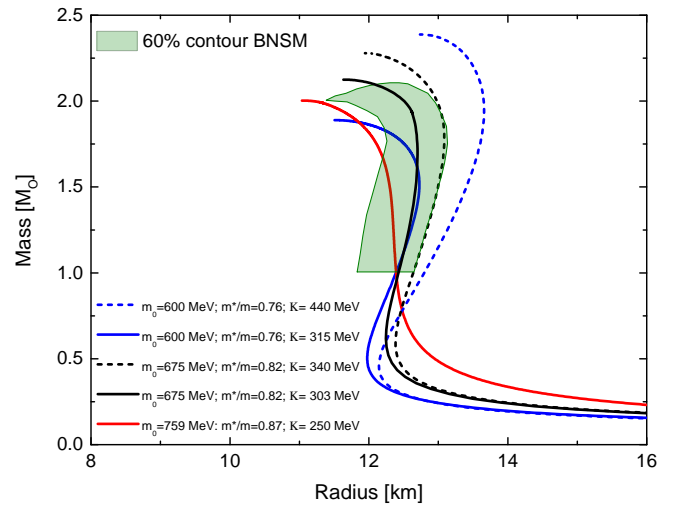


Figure 3. (Color online) Neutron star M-R curves for the different EoS's used. The solid black line gives the best agreement. Too stiff EoS give too large radii and too strong momentum dependencies too small maximum masses.

## II. RESULTS FROM HIC

In heavy ion collisions the equation of state is mostly inferred through the directed  $v_1$  and elliptic flow  $v_2$ , being the first and second order Fourier coefficient in the expansion of the azimuthal angular distribution [35], of protons [36, 37]. In the energy regime probed with the SIS18 accelerator the generation of elliptic flow follows an intricate interplay of interactions via the potential and collisions [38]. The HADES experiment at GSI has recently measured highly differential data of proton and light nuclei elliptic flow [39, 40]. To relate the different CMF parametrizations to the heavy ion data by HADES, we will employ the UrQMD model which has recently been extended to incorporate a momentum dependent potential from CMF [22]. Since the procedure has not been changed in the current work we refer to [22] for the description of the model.

In figure 4 (upper panel) we compare results of proton elliptic flow calculated with the different parametrizations of the CMF as a function of transverse momentum  $p_T$  in 20–30% peripheral Au+Au collisions with the recent HADES measurements. The colors and styles of the lines are the same as in the previous figures. Very clearly the best fitting parametrization obtained from neutron star mass-radius constraints also yields the best description of proton elliptic flow data in 20–30% peripheral AuAu collisions at 1.23A GeV kinetic beam energy. In comparison to the other parametrizations one can conclude that a larger incompressibility turns  $v_2$  more negative, as well as does a stronger momentum dependence. As a second step we use the best fitting parametrization to evaluate the elliptic flow as a function of transverse momentum for 4 different centrality classes shown in figure

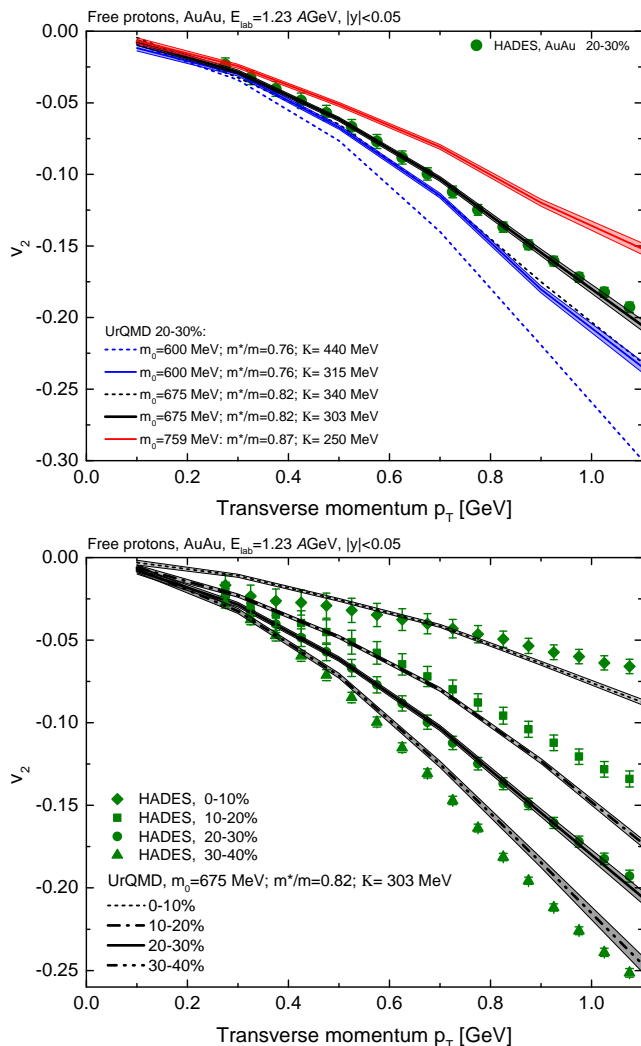


Figure 4. (Color online) Proton  $v_2$  as function of transverse momentum for the different EoS (upper plot) and for the best fitting EoS (black line) for different centralities compared to HADES data (lower plot).

4 (lower panel). The results show a good agreement between the UrQMD model calculations using the best fitting parametrization of the CMF with measured data on elliptic flow.

In addition to flow observables, the production of strange hadrons, specifically Kaons, was shown to be sensitive to the equation of state. While the total yield of Kaons and hyperons depends on both, the equation of state as well as the momentum dependence of the corresponding potentials, the centrality dependence of Kaon production was shown to be sensitive only on the equation of state [41–44]. Figure 5 (upper panel) shows the rapidity distributions of  $\Lambda$ 's for two different centrality bins, using the five CMF parametrizations discussed above. The hyperon rapidity distribution shows a very strong sensitivity to the momentum dependence as well as the equation of state. One clearly observes again, that

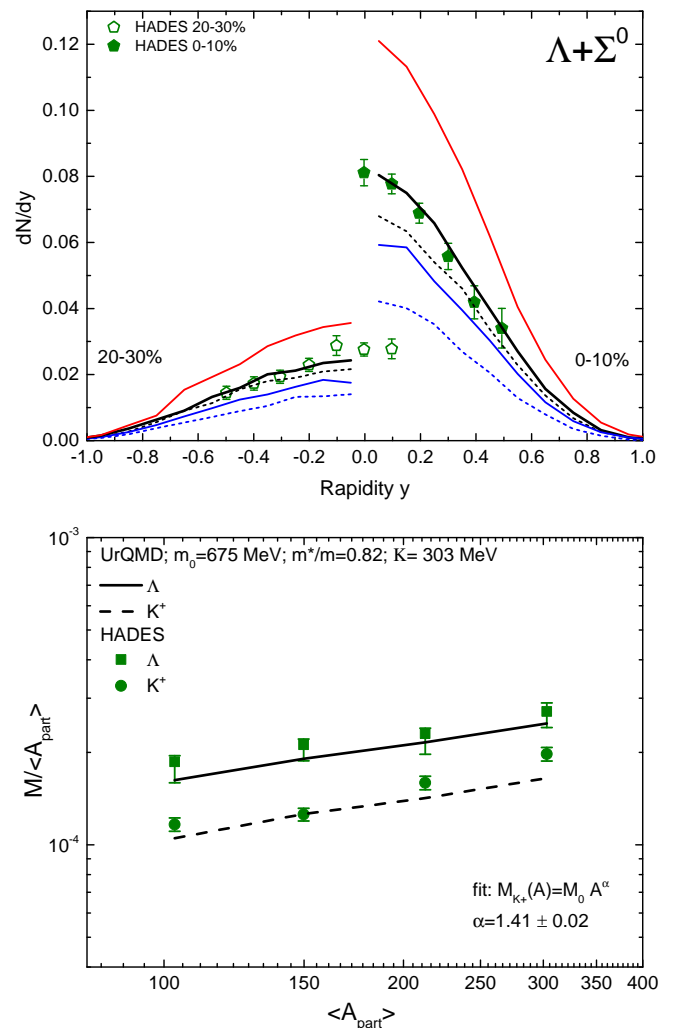


Figure 5. (Color online)  $\Lambda$  and  $K^+$  rapidity distributions compared to HADES data (upper plot). The centrality dependence of kaon production (lower plot) is consistent with HADES data.

the best-fit parametrization shown as black line gives the best description of the HADES data [45] for both centrality bins. To quantify the centrality dependence we show the integrated multiplicities of  $K^+$  and  $\Lambda$ , scaled by the number of participants according to a Glauber fit [45], as function of the number of participants. This dependence can be fitted with a simple parametrization:

$$M_{K^+}(A) = M_0 A^\alpha \quad (3)$$

where  $M_0$  is a normalization constant and  $\alpha$  has been shown to be sensitive to the density dependence of the equation of state. Using our best fitting CMF parameter set we obtain a value of  $\alpha = 1.41 \pm 0.02$  which agrees well with the HADES result as well with previous results from the KaoS and FOPI collaborations [46, 47].

In addition to the Kaon number, the pion number was

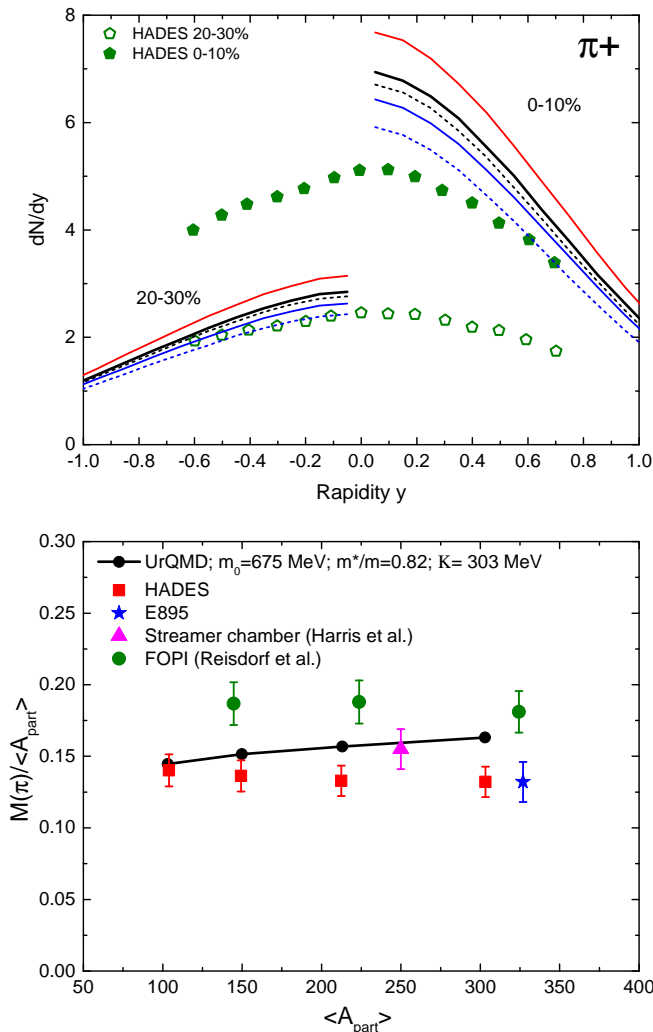


Figure 6. (Color online) Pion rapidity distributions compared to HADES data (upper plot). The centrality dependence is consistent with world data (lower plot).

also shown to be a sensitive probe of the momentum dependence of the potential [48, 49]. Recent HADES data however have been overestimated by essentially all baseline transport model simulations [50]. Figure 6 (upper panel) shows a comparison of the positively charged pion  $dN/dy$  from or simulations with the published HADES data in two different centrality bins. As one can see none of the momentum dependences is able to describe the pion multiplicities well, especially for central collisions. A more balanced picture emerges as one compares the centrality dependence of the pion production of different experiments with the best fitting parametrization (black) in the lower panel of figure 6. Again, one observes that the best-fit is compatible with the available data within their errors.

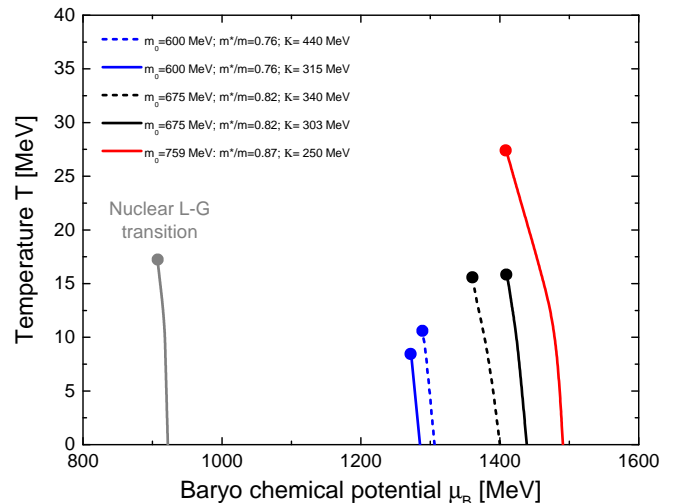


Figure 7. (Color online) Different phase diagrams for the various parametrizations. A larger momentum dependence tends to decrease the critical chemical potential and temperature.

### III. DISCUSSION

It was shown how a consistent description of the equation of state (and momentum dependence of the nuclear potential) can be achieved for the description of neutron star properties as well as heavy ion reactions. To do so we used the Chiral Mean Field Model to calculate several parametrizations of the iso-spin symmetric as well as neutron star equation of state. The parameters of the model were fixed by new constraints on the mass-radius relation from neutron stars. The resulting equation of state is able to describe several experimentally measured observable sensitive to the equation of state and momentum dependence. A small discrepancy in the pion production at the HADES experiment is still visible.

The resulting parameters of the best fit can be used to draw a corresponding phase diagram of dense matter which is shown in figure 7. The well known nuclear liquid-gas transition is shown as grey line. The different colored lines correspond to the chiral transitions in the CMF for the different parameter sets used in our study. The black solid line corresponds to the best fitting curve. Due to the large repulsion at high densities in the CMF model, the critical endpoint for all the scenarios is rather low  $T_{CEP} < 30$  MeV. The values for the best fitting parametrization are :  $T_{CEP} = 16$  MeV and  $\mu_{CEP} = 1410$  MeV.

The current analysis presents a way forward in how results from astrophysical observations like neutron star masses and binary neutron star mergers can be combined with heavy ion observables to constrain the high density and temperature QCD equation of state. It also shows a path forward on how such analyses can and should be improved in several ways in the future. This includes the implementation of an explicit dependence of the equa-

tion of state on the scalar density, and thus the temperature, which would be naturally included in a relativistic description of the MD-part with a scalar and vector density. In addition the iso-spin dependence of the EoS can be easily and consistently implemented in our model through the CMF. Finally, a more complete set of data, including results from other experiments can be used in a statistical inference that can constrain the CMF parameters in a more quantitative way that also includes uncertainties.

## ACKNOWLEDGMENTS

J.S. and T.R. thank the Lawrence Berkeley Lab for its hospitality and Volker Koch for helpful discussions. T.R. acknowledges support through the Main-Campus-Doctus fellowship provided by the Stiftung Polytechnische Gesellschaft Frankfurt am Main (SPTG). T.R. thanks the Samson AG for their support. M.O.K. was supported by the ErUM-Data funding line from BMBF through the KISS project. The computational resources for this project were provided by the Center for Scientific Computing of the GU Frankfurt and the Goethe-HLR.

- 
- [1] S. Borsanyi, Z. Fodor, C. Hoelbling, S. D. Katz, S. Krieg, C. Ratti, and K. K. Szabo (Wuppertal-Budapest), *JHEP* **09**, 073 (2010), arXiv:1005.3508 [hep-lat].
- [2] A. Bazavov *et al.*, *Phys. Rev. D* **85**, 054503 (2012), arXiv:1111.1710 [hep-lat].
- [3] A. Bazavov *et al.*, *Phys. Rev. D* **95**, 054504 (2017), arXiv:1701.04325 [hep-lat].
- [4] S. Borsanyi, Z. Fodor, J. N. Guenther, R. Kara, S. D. Katz, P. Parotto, A. Pasztor, C. Ratti, and K. K. Szabo, *Phys. Rev. Lett.* **125**, 052001 (2020), arXiv:2002.02821 [hep-lat].
- [5] A. Bazavov *et al.* (HotQCD), *Phys. Lett. B* **795**, 15 (2019), arXiv:1812.08235 [hep-lat].
- [6] V. Vovchenko, J. Steinheimer, O. Philipsen, and H. Stoecker, *Phys. Rev. D* **97**, 114030 (2018), arXiv:1711.01261 [hep-ph].
- [7] C. S. Fischer, J. Luecker, and C. A. Welzbacher, *Phys. Rev. D* **90**, 034022 (2014), arXiv:1405.4762 [hep-ph].
- [8] W.-j. Fu, J. M. Pawlowski, and F. Rennecke, *Phys. Rev. D* **101**, 054032 (2020), arXiv:1909.02991 [hep-ph].
- [9] F. Gao and J. M. Pawlowski, *Phys. Rev. D* **102**, 034027 (2020), arXiv:2002.07500 [hep-ph].
- [10] P. J. Gunkel and C. S. Fischer, *Phys. Rev. D* **104**, 054022 (2021), arXiv:2106.08356 [hep-ph].
- [11] M. Hippert, J. Grefa, T. A. Manning, J. Noronha, J. Noronha-Hostler, I. Portillo Vazquez, C. Ratti, R. Rougemont, and M. Trujillo, *Phys. Rev. D* **110**, 094006 (2024), arXiv:2309.00579 [nucl-th].
- [12] G. Basar, *Phys. Rev. C* **110**, 015203 (2024), arXiv:2312.06952 [hep-th].
- [13] D. A. Clarke, P. Dimopoulos, F. Di Renzo, J. Goswami, C. Schmidt, S. Singh, and K. Zambello, *PoS LAT-TICE2023*, 168 (2024), arXiv:2401.08820 [hep-lat].
- [14] A. Sorensen and P. Sorensen, (2024), arXiv:2405.10278 [nucl-th].
- [15] H. Shah, M. Hippert, J. Noronha, C. Ratti, and V. Vovchenko, (2024), arXiv:2410.16206 [hep-ph].
- [16] M. Bluhm *et al.*, *Nucl. Phys. A* **1003**, 122016 (2020), arXiv:2001.08831 [nucl-th].
- [17] M. Nahrgang, S. Leupold, C. Herold, and M. Bleicher, *Phys. Rev. C* **84**, 024912 (2011), arXiv:1105.0622 [nucl-th].
- [18] P. Papazoglou, D. Zschesche, S. Schramm, J. Schaffner-Bielich, H. Stoecker, and W. Greiner, *Phys. Rev. C* **59**, 411 (1999), arXiv:nucl-th/9806087.
- [19] J. Steinheimer, S. Schramm, and H. Stoecker, *J. Phys. G* **38**, 035001 (2011), arXiv:1009.5239 [hep-ph].
- [20] A. Motornenko, J. Steinheimer, V. Vovchenko, S. Schramm, and H. Stoecker, *Phys. Rev. C* **101**, 034904 (2020), arXiv:1905.00866 [hep-ph].
- [21] J. Steinheimer, S. Schramm, and H. Stoecker, *Phys. Rev. C* **84**, 045208 (2011), arXiv:1108.2596 [hep-ph].
- [22] J. Steinheimer, T. Reichert, Y. Nara, and M. Bleicher, (2024), arXiv:2410.01742 [hep-ph].
- [23] S. Hama, B. C. Clark, E. D. Cooper, H. S. Sherif, and R. L. Mercer, *Phys. Rev. C* **41**, 2737 (1990).
- [24] K. Weber, B. Blaettel, W. Cassing, H. C. Doenges, V. Koch, A. Lang, and U. Mosel, *Nucl. Phys. A* **539**, 713 (1992).
- [25] J. R. Oppenheimer and G. M. Volkoff, *Phys. Rev.* **55**, 374 (1939).
- [26] G. A. Lalazissis, T. Niksic, D. Vretenar, and P. Ring, *Phys. Rev. C* **71**, 024312 (2005).
- [27] S. Altiparmak, C. Ecker, and L. Rezzolla, *Astrophys. J. Lett.* **939**, L34 (2022), arXiv:2203.14974 [astro-ph.HE].
- [28] M. C. Miller *et al.*, *Astrophys. J. Lett.* **887**, L24 (2019), arXiv:1912.05705 [astro-ph.HE].
- [29] T. E. Riley *et al.*, *Astrophys. J. Lett.* **887**, L21 (2019), arXiv:1912.05702 [astro-ph.HE].
- [30] G. Raaijmakers *et al.*, *Astrophys. J. Lett.* **887**, L22 (2019), arXiv:1912.05703 [astro-ph.HE].
- [31] M. C. Miller *et al.*, *Astrophys. J. Lett.* **918**, L28 (2021), arXiv:2105.06979 [astro-ph.HE].
- [32] T. E. Riley *et al.*, *Astrophys. J. Lett.* **918**, L27 (2021), arXiv:2105.06980 [astro-ph.HE].
- [33] G. Raaijmakers, S. K. Greif, K. Hebeler, T. Hinderer, S. Nissanke, A. Schwenk, T. E. Riley, A. L. Watts, J. M. Lattimer, and W. C. G. Ho, *Astrophys. J. Lett.* **918**, L29 (2021), arXiv:2105.06981 [astro-ph.HE].
- [34] B.-A. Li, B.-J. Cai, W.-J. Xie, and N.-B. Zhang, *Universe* **7**, 182 (2021), arXiv:2105.04629 [nucl-th].
- [35] S. Voloshin and Y. Zhang, *Z. Phys. C* **70**, 665 (1996), arXiv:hep-ph/9407282.
- [36] J. Steinheimer, A. Motornenko, A. Sorensen, Y. Nara, V. Koch, and M. Bleicher, *Eur. Phys. J. C* **82**, 911 (2022), arXiv:2208.12091 [nucl-th].
- [37] A. Sorensen *et al.*, *Prog. Part. Nucl. Phys.* **134**, 104080 (2024), arXiv:2301.13253 [nucl-th].
- [38] T. Reichert and J. Aichelin, (2024), arXiv:2411.12908 [nucl-th].
- [39] J. Adamczewski-Musch *et al.* (HADES), *Phys. Rev. Lett.* **125**, 262301 (2020), arXiv:2005.12217 [nucl-ex].

- [40] J. Adamczewski-Musch *et al.* (HADES), *Eur. Phys. J. A* **59**, 80 (2023), [arXiv:2208.02740 \[nucl-ex\]](#).
- [41] C. Hartnack, H. Oeschler, Y. Leifels, E. L. Bratkovskaya, and J. Aichelin, *Phys. Rept.* **510**, 119 (2012), [arXiv:1106.2083 \[nucl-th\]](#).
- [42] C. Hartnack, H. Oeschler, and J. Aichelin, *Phys. Rev. Lett.* **96**, 012302 (2006), [arXiv:nucl-th/0506087](#).
- [43] C. Hartnack, L. Sehn, J. Jaenicke, H. Stoecker, and J. Aichelin, *Nucl. Phys. A* **580**, 643 (1994).
- [44] C. Hartnack, J. Aichelin, H. Stoecker, and W. Greiner, *Phys. Rev. Lett.* **72**, 3767 (1994).
- [45] J. Adamczewski-Musch *et al.* (HADES), *Phys. Lett. B* **793**, 457 (2019), [arXiv:1812.07304 \[nucl-ex\]](#).
- [46] A. Forster *et al.*, *Phys. Rev. C* **75**, 024906 (2007), [arXiv:nucl-ex/0701014](#).
- [47] N. Bastid *et al.* (FOPI), *Phys. Rev. C* **76**, 024906 (2007), [arXiv:nucl-ex/0703036](#).
- [48] J. Aichelin, A. Rosenhauer, G. Peilert, H. Stoecker, and W. Greiner, *Phys. Rev. Lett.* **58**, 1926 (1987).
- [49] J. Hong and P. Danielewicz, *Phys. Rev. C* **90**, 024605 (2014), [arXiv:1307.7654 \[nucl-th\]](#).
- [50] J. Adamczewski-Musch *et al.* (HADES), *Eur. Phys. J. A* **56**, 259 (2020), [arXiv:2005.08774 \[nucl-ex\]](#).